Pyruvate kinase M knockdown–induced signaling via AMP-activated protein kinase promotes mitochondrial biogenesis, autophagy, and cancer cell survival

Received for publication, April 14, 2017, and in revised form, August 1, 2017 Published, Papers in Press, August 4, 2017, DOI 10.1074/jbc.M117.791343

Gopinath Prakasam[‡], Rajnish Kumar Singh[‡§], Mohammad Askandar Iqbal[‡¶], Sunil Kumar Saini[‡], Ashu Bhan Tiku[‖], and Rameshwar N. K. Bamezai[‡1]

From the [‡]School of Life Sciences and [‖]Radiation and Cancer Therapeutics Laboratory, School of Life Sciences, Jawaharlal Nehru University, New Delhi 110067, India, [§]Department of Microbiology and Tumor Virology Program of the Abramson Cancer Center, Perelman School of Medicine, University of Pennsylvania, Philadelphia, Pennsylvania 19104, and [¶]Department of Biotechnology, Faculty of Natural Sciences, Jamia Millia Islamia, New Delhi 110025, India

Edited by Alex Toker

Preferential expression of the low-activity (dimeric) M2 isoform of pyruvate kinase (PK) over its constitutively active splice variant M1 isoform is considered critical for aerobic glycolysis in cancer cells. However, our results reported here indicate co-expression of PKM1 and PKM2 and their possible physical interaction in cancer cells. We show that knockdown of either PKM1 or PKM2 differentially affects net PK activity, viability, and cellular ATP levels of the lung carcinoma cell lines H1299 and A549. The stable knockdown of PK isoforms in A549 cells significantly reduced the cellular ATP level, whereas in H1299 cells the level of ATP was unaltered. Interestingly, the PKM1/2 knockdown in H1299 cells activated AMP-activated protein kinase (AMPK) signaling and stimulated mitochondrial biogenesis and autophagy to maintain energy homeostasis. In contrast, knocking down either of the PKM isoforms in A549 cells lacking LKB1, a serine/threonine protein kinase upstream of AMPK, failed to activate AMPK and sustain energy homeostasis and resulted in apoptosis. Moreover, in a similar genetic background of silenced PKM1 or PKM2, the knocking down of AMPKα1/2 catalytic subunit in H1299 cells induced apoptosis. Our findings help explain why previous targeting of PKM2 in cancer cells to control tumor growth has not met with the expected success. We suggest that this lack of success is because of AMPK-mediated energy metabolism rewiring, protecting cancer cell viability. On the basis of our observations, we propose an alternative therapeutic strategy of silencing either of the PKM isoforms along with AMPK in tumors.

Cancer cells acquire a unique metabolic signature of aerobic glycolysis (Warburg effect) and undergo metabolic fine-tuning to feast on glucose and excrete a major chunk as lactate (1). Although our understanding of the Warburg effect (aerobic glycolysis) is still inconclusive, the growing body of evidence highlights that the rewiring of cancer metabolism confers a multitude of advantages, including macromolecular synthesis, rapid ATP generation, and maintaining redox balance (2, 3). The M2 isoform of pyruvate kinase (PKM2)[2], a glycolytic terminal enzyme and one of the two alternate isoforms encoded by *PKM* gene, has emerged as a key factor that regulates aerobic glycolysis in cancer cells (4, 5). The expression of PKM isoforms has been assumed as mutually exclusive in nature, where of 12 exons that the *PKM* gene harbors, a primary transcript that retains Exon 9 and skips Exon 10 is the M1 isoform of pyruvate kinase (PKM1) and the one that retains Exon 10 is PKM2 (6). A preferential expression of PKM2 over other tissue-specific PK isoforms has been proposed as one of the metabolic hallmarks of cancer (3, 8), in which preferential expression of PKM2 and its enzymatically inactive dimeric state serve a pivotal role in cancer growth by governing aerobic glycolysis (5, 9–13).

In addition to aerobic glycolysis, PKM2 provides multiple benefits to cancer cells by performing the nonmetabolic role of co-transcriptional activation (14–16), protein kinase function (17, 18), and chromosomal segregation (19). Supporting such a deep-rooted association with cancer, the M2 isoform of pyruvate kinase has emerged as a potential candidate to target different types of tumors. The strategies of PKM2 inhibition or silencing (4, 20–22) and activation (23–25) have been equally debated in literature for their therapeutic potential in inhibiting tumor growth. However, recent studies have highlighted the limitation that exists in the strategy of targeting PKM2 in cancer. The knockdown of PKM2 *in vitro* and *in* vivo has been reported to affect proliferation and viability of cancer cells of different tissue origin heterogeneously (4, 20, 26, 27). To find out what determines such a heterogeneous response, we sought to examine the key features that confer protection against PKM2 knockdown–induced growth inhibition and cell death in cancer cells. A deep insight, we expected, would rationalize a

This work was supported in part by Government of India, University Grant Commission Grant F. No 17–4/2001 (NS/PE), provided to the National Centre for Applied Human Genetics (NCAHG) for up to March 2012. This work was also supported by a meritorious science research fellowship from University Grant Commission, Government of India (to G. P.). The authors declare that they have no conflicts of interest with the contents of this article.

This article contains supplemental Tables S1 and S2.

[1] To whom correspondence should be addressed. Fax: 91-11-26742211. E-mail: bamezai@hotmail.com.

[2] The abbreviations used are: PKM2, M2 isoform of pyruvate kinase; PK, pyruvate kinase; AMPK, AMP-activated protein kinase; LC-MS, liquid chromatography-mass spectrometry; IP, immunoprecipitation; mTOR, mammalian target of rapamycin; CCK8, Cell Counting Kit-8; PARP, poly(ADP-ribose) polymerase.

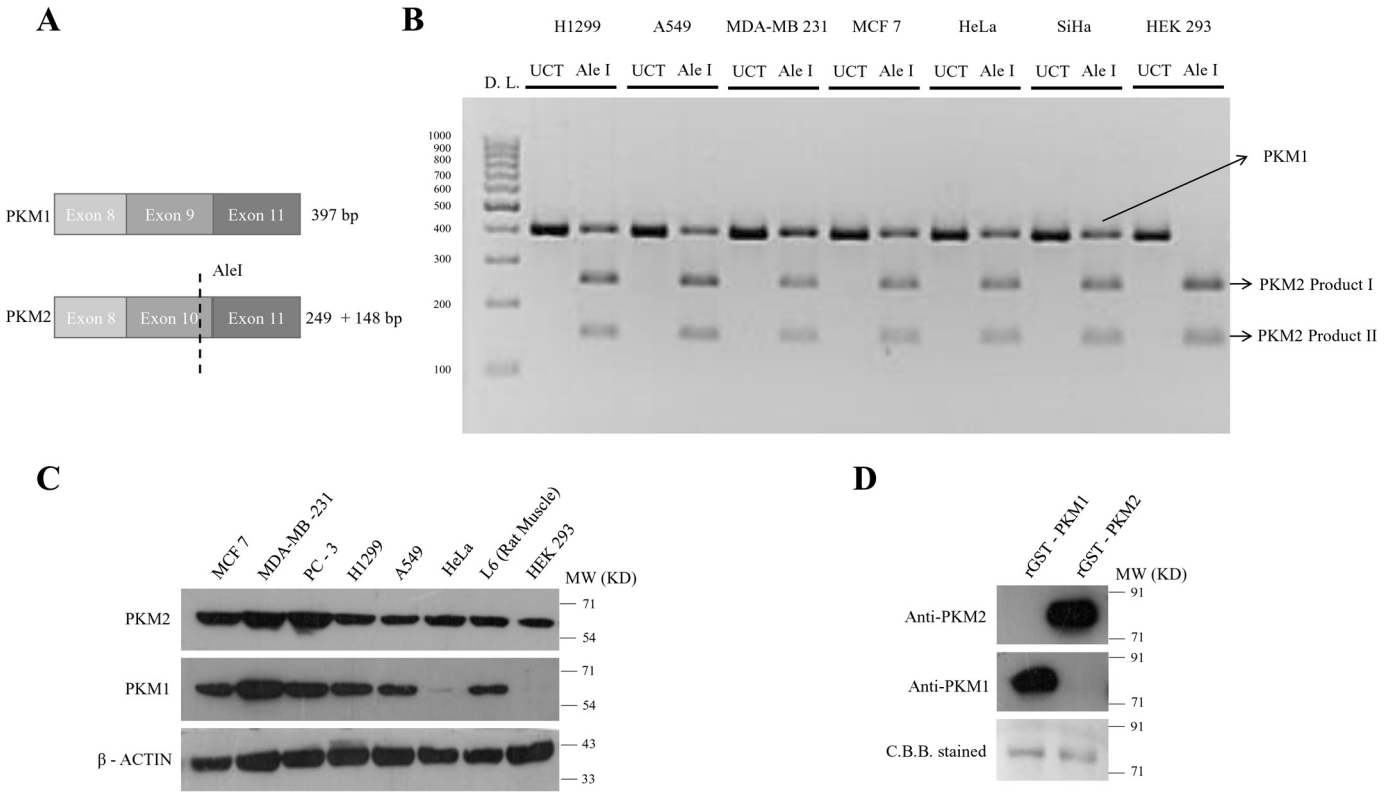

Figure 1. Co-expression of PKM1 and PKM2 in cancer cell lines. *A*, schematic representation to depict the approach employed to assay PKM1/PKM2 mRNA ratio in human cancer cells as in *B*. *B*, semi-quantitative RT-PCR followed by PKM2 exon-specific restriction digestion with Ale I restriction enzyme to examine the proportion of PKM1 and PKM2 expression in human cancer cells. *UCT*, uncut; *Ale I*, restriction digested, and *D.L.*, DNA Ladder. Uncut PKM1 and PKM2 397 bp, Ale I undigested PKM1 397 bp, Ale I digested PKM2 product I (249 bp), and Ale I digested PKM2 product II (148 bp). *C*, immunoblots of PKM1 and PKM2 to demonstrate co-expression of PKM1 and PKM2 isoforms in six human cancer cell lines of four different tissue origins and two noncancerous cell lines, used as a control. *D*, immunoblotting with anti-PKM1 and anti-PKM2 to show the specificity for purified recombinant PKM1 (rGST-PKM1) and PKM2 (rGST-PKM1), stained with Coomassie Brilliant Blue (*C.B.B.*).

promising therapeutic strategy, as proposed here. We proposed to answer some of these contradictions and suggest the importance of both the isoforms of *PKM* gene in relation to cancer metabolism and growth. Further, we demonstrated that the knockdown of PKM2 or PKM1 perturbed cellular ATP level and activated AMPK in cancer cells that expressed functional LKB1. Activated AMPK, to restore energy homeostasis, stimulated mitochondrial biogenesis and autophagy. We have shown that the knockdown of AMPK in cells silenced for PKM2 or PKM1 showed growth inhibition and resulted in apoptosis. Together, our results suggest how important it is to target the reprogramming of the energy metabolism of a cancer cell to break its vicious cycle of turning resistant to therapies that perturb ATP level.

Results

Cancer cells co-express M1 and M2 isoforms of pyruvate kinase and localize differentially to subcellular organelles

The phenomenon of co-expression was noticed at RNA level in cultured human cancer cells, using semi-quantitative RT-PCR followed by exon-specific restriction digestion of PKM2, a modified technique adopted from David *et al.* (49), to examine the proportion of the expression of the PKM1 and PKM2 isoforms (Fig. 1, *A* and *B*). The co-expression of the two isoforms was also observed by Western blot analysis in six different cell lines (MCF-7, MDA-MB-231, PC-3, H1299, A549, and HeLa) derived from four different tissue origins (breast, lung, prostate, and cervical) along with two other noncancerous cell lines (L6 (rat skeletal muscle) and HEK293 (human embryonic kidney)) (Fig. 1*C*). These observations were also validated using stage-specific sporadic breast tumors and the adjoining normal tissues (data not shown). To ensure that the antibodies used for the two isoforms were not cross-reacting, the recombinant GST–tagged PKM1 and PKM2 proteins were used to validate their specificity (Fig. 1*D*).

To identify the protein-interacting partners of PKM1 isoform, we generated H1299 stable cells expressing Myc-tagged PKM1 (PKM1-Myc-His) (Fig. 2*A*). Further, the complex of PKM1 and its interacting partners were co-purified by Myc-tag immunoprecipitation from whole cell lysates of H1299 stable cells and subjected to liquid chromatography-mass spectrometry (LC-MS)– based analysis. From the results of two independent LC-MS studies, we found nearly 30 interacting proteins of PKM1 (Fig. 2*B* and supplemental Table S1), which involved the proteins from cytoplasm, mitochondria, and nucleus, as an integral part of diverse cellular machinery of glycolytic pathway, mitochondrial electron transport chain, protein translation, protein folding, DNA replication, and cytoskeletal networks (Fig. 2*B*). To support the observation of PKM1 interaction with proteins of different subcellular organelles, we analyzed the amino acid sequence of PKM1, using six online computational tools to predict PKM1 subcellular localization and compared with PKM2. The predictions revealed that both PKM1 and PKM2 localized predominantly in the cytoplasm,

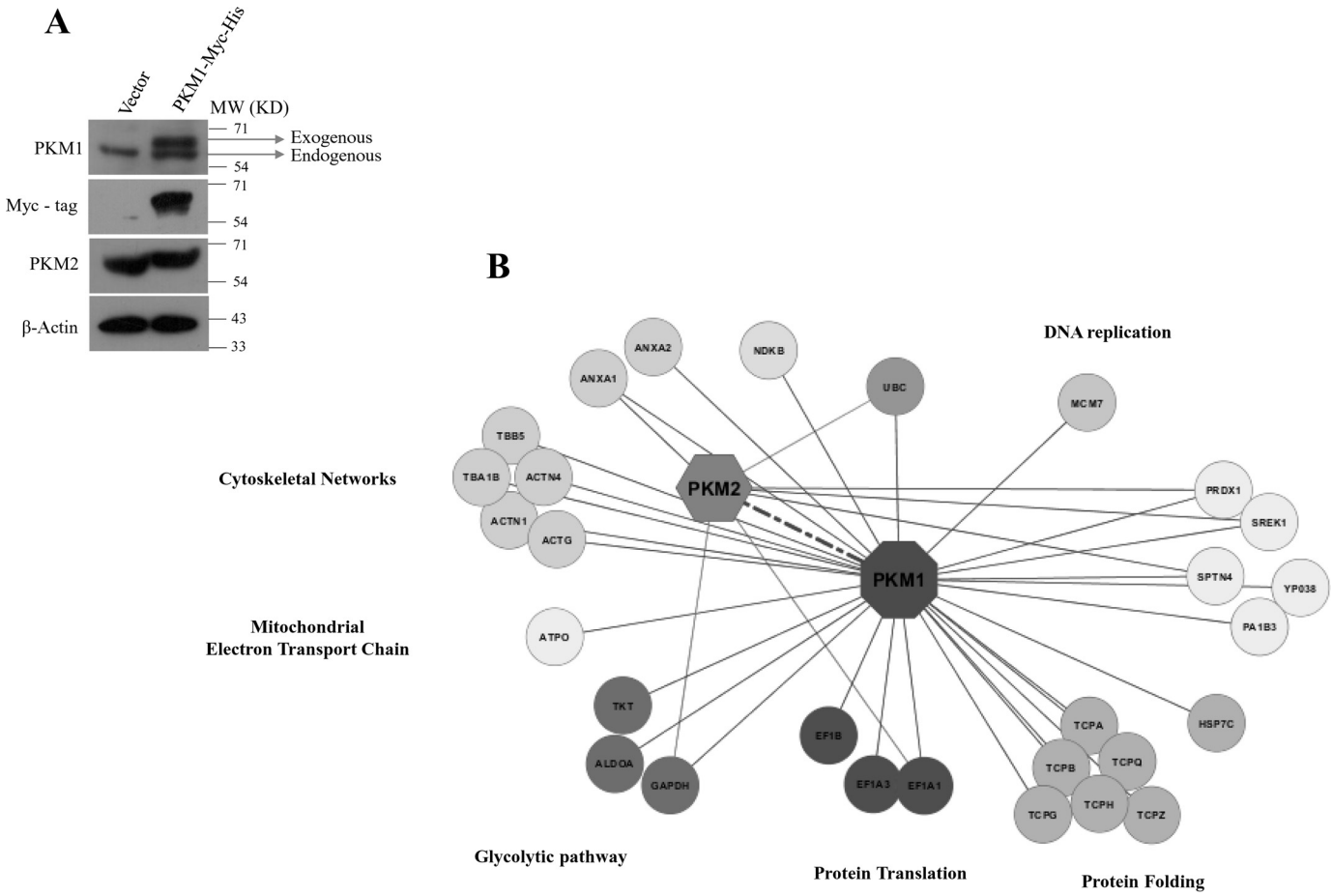

Figure 2. Identification of protein interacting partners of human PKM1 using LC-MS-MS. *A*, immunoblots of Myc-His–tagged PKM1 and PKM2 from the protein lysates of H1299 stable cells, transfected with empty vector or Myc-His–tagged PKM1 cDNA. *B*, cytoscape map of PKM1 interactome, involving a total of 30 interacting partners of PKM1, co-immunoprecipitated with Myc-tagged PKM1 from H1299 lysate and identified using LC-MS-MS from two biological replicates. The identified interacting partners were further separated with distinct color codes and were marked as entities that were an integral part of cellular machinery, such as glycolytic pathway, mitochondrial electron transport chain, protein translational, protein folding, DNA replication, and cytoskeletal networks.

followed by their presence in mitochondria and at appreciative levels in the nucleus (supplemental Table S2). This was further confirmed by immunoblot studies with subcellular fractions and confocal microscopy. Results revealed a differential localization pattern of PKM isoforms in H1299 and A549 cells, where PKM1 localized within the cytosol, mitochondria, and nucleus. PKM2, however, localized predominantly in the cytoplasm and with appreciative levels in the nucleus, showed an apparent absence in the mitochondria (Fig. 3, *A*–*F*). Interestingly, the interactome data of PKM1 revealed a possible interaction between co-expressed PKM1 and PKM2 isoforms, where LC-MS data of PKM1 isoform exhibited the peptide sequence corresponding to that of PKM2 isoform. To validate the interaction between PKM1 and PKM2, we carried out co-immunoprecipitation (co-IP) and confocal microscopy studies. The IP of Myc-tag from the lysate of H1299 cells stably expressing PKM1-Myc showed the co-precipitation of endogenous PKM2, reconfirming the interaction between the two. This was further validated in the reciprocal experiment between exogenously expressing PKM2-Myc and endogenous PKM1 (Fig. 4*A*). The distribution and strong interaction within cytoplasm between the endogenous PKM1 (immunostained with anti-PKM1 and Alexa Fluor 594 (red)) and exogenously expressed Myc-tagged PKM2 (PKM2-Myc) (immunostained with anti-Myc and Alexa Fluor 488 (green)) were visualized using confocal microscopy (Fig. 4*B*). The likelihood of the hetero-oligomers, expected to be formed through PKM1–PKM2 interaction, was further examined by separating PKM oligomers (dimer and tetramer) from H1299 cell lysates in a glycerol step gradient subjected to ultracentrifugation (10, 12) and examining the pyruvate kinase activity (Fig. 4*C*), followed by Western blot analysis of the same glycerol fraction with PKM1- and PKM2-specific antibodies. This established the formation of heterotetramers of PKM1 and PKM2, where heterodimers were not detected (Fig. 4*D*). Further, to understand the relevance of the co-expression of the PKM1 isoform, we proposed to study its role in aerobic glycolysis and cell viability using lung cancer cell lines.

PKM1 or PKM2 knockdown differentially affects net pyruvate kinase activity, aerobic glycolysis, ATP level, and cell viability

To knock down the expression of PKM isoforms, we introduced the lentivirus harboring shRNA, targeting PKM1 or PKM2 mRNA in human lung cancer cell lines (A549 and H1299), followed by selection to generate stably transduced cells. PKM1 or PKM2 knockdown was validated with Western blot analysis (Fig. 5*A*). When measured for PK activity, H1299

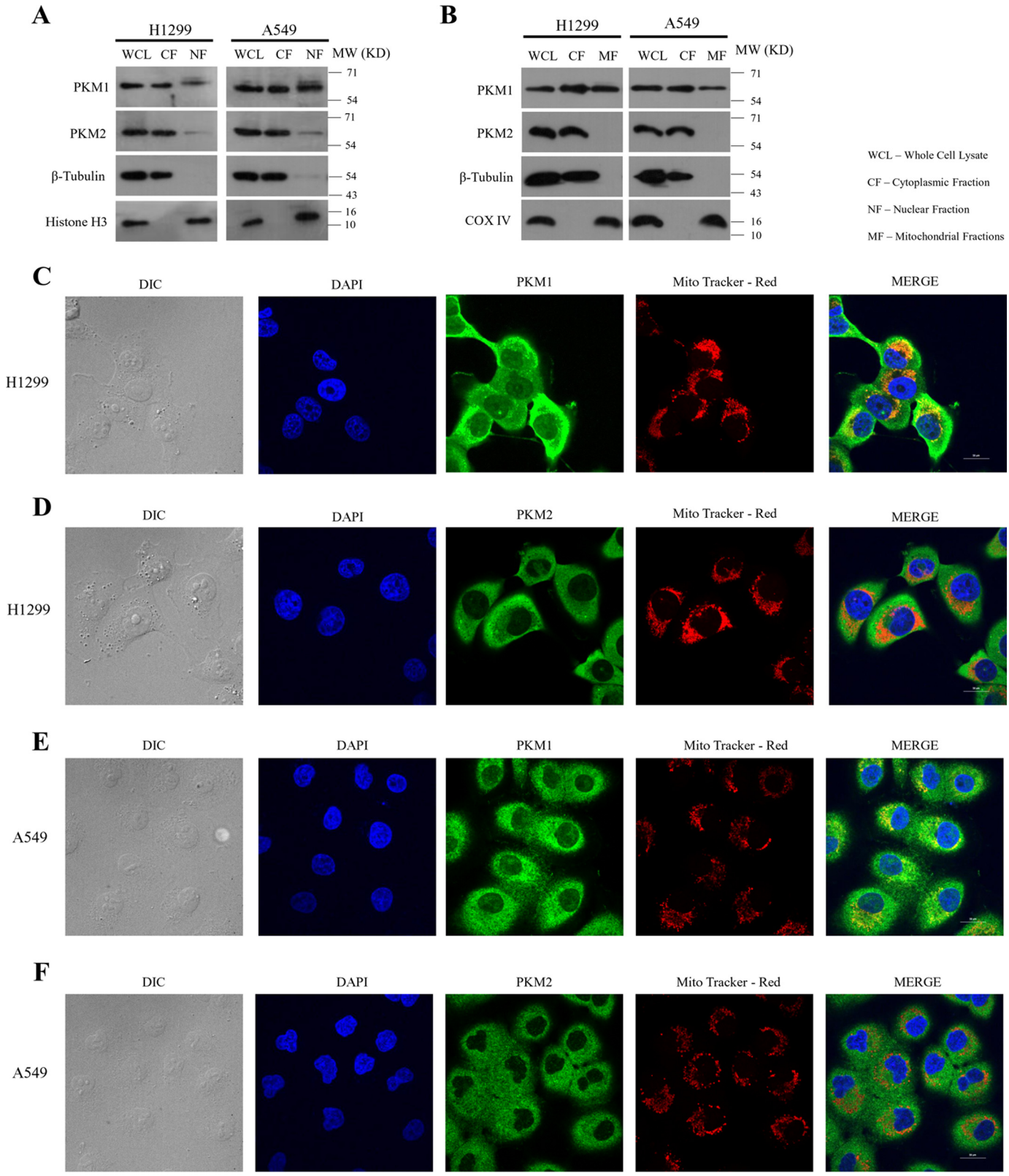

Figure 3. Subcellular localization of PKM isoforms and their validation. *A*, immunoblots of PKM1 and PKM2 from the lysate of H1299 (*left panel*) and A549 (*right panel*) cells collected by fractionating the cytoplasm and the nucleus (*WCL*, whole cell lysate; *CF*, cytoplasmic fraction; and *NF*, nuclear fraction). PARP and β-tubulin served as loading controls for nucleus, and cytoplasm respectively. *B*, immunoblots of PKM1 and PKM2 from lysate of H1299 (*left panel*) and A549 (*right panel*) cells collected by fractionating the cytoplasm and the mitochondria (*WCL*, whole cell lysate; *CF*, cytoplasmic fraction; *MF*, mitochondrial fraction). COX IV and β-tubulin served as loading controls for mitochondria and cytoplasm, respectively. *C–F*, confocal microscopy images demonstrating the subcellular localization of PKM1 or PKM2 in H1299 and A549 cells, immunostained with antibodies of PKM2 (*green*) or PKM1 (*green*), mitochondria stained with Mito-tracker Red (*red*) and the nucleus was stained with DAPI (*blue*). Merged figures are shown with a *scale bar* of 20 μm.

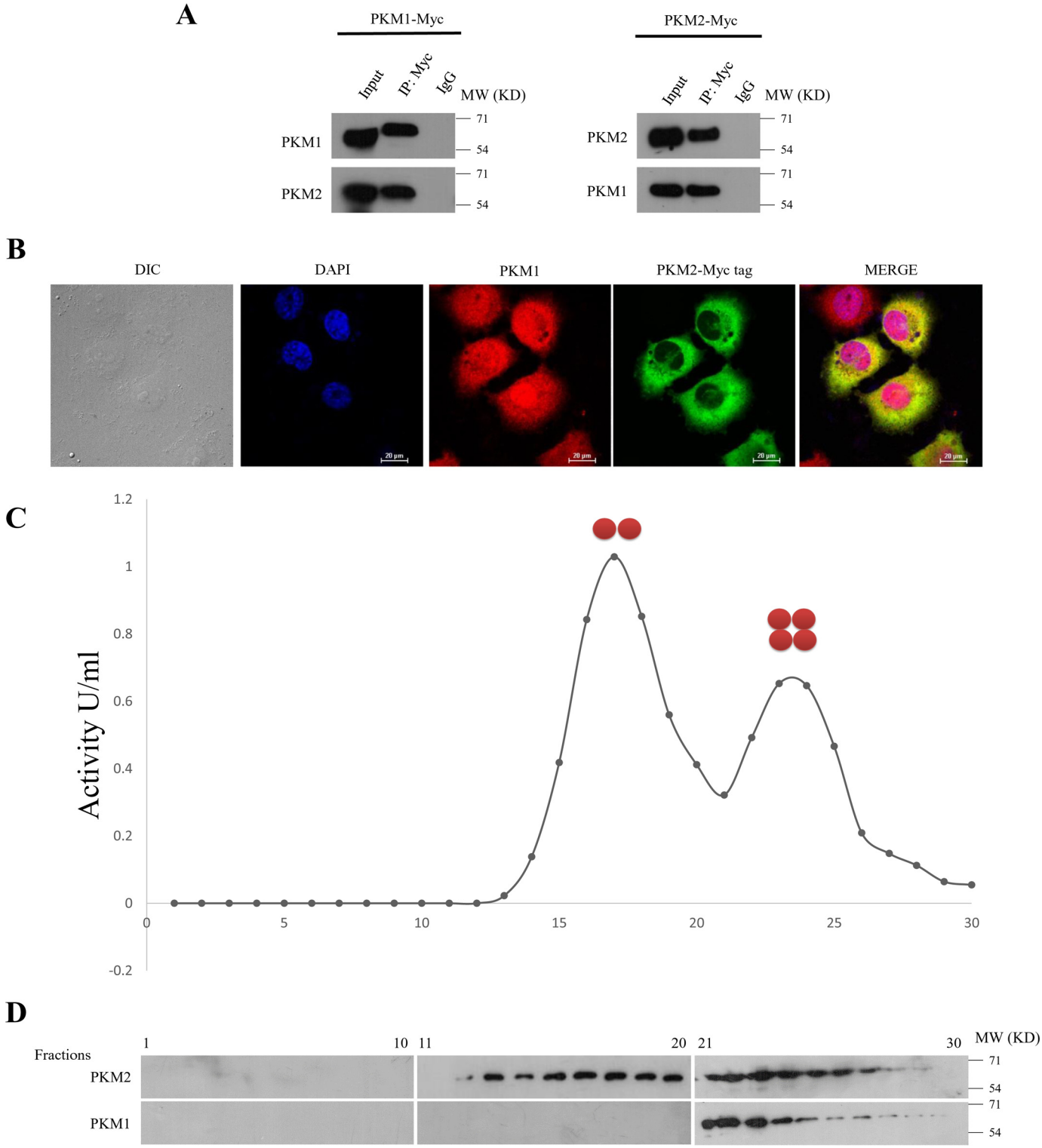

Figure 4. PKM1 and PKM2 interact with each other. *A*, immunoprecipitation (IP) performed with anti-Myc-tag in lysates of H1299 cells, stably expressing Myc-tagged PKM1 (PKM1-Myc) (*left panel*), or Myc-tagged PKM2 (PKM2-Myc) (*right panel*), followed by immunoblotting with PKM1 or PKM2 antibodies, to show the interaction between PKM-isoforms (IgG used as isotype control). *B*, confocal microscopy images, displaying the co-localization of endogenous PKM1 (immunostained with anti-PKM1 and secondary anti-Alexa Fluor 589 red) and exogenously expressed Myc-tagged PKM2 (immunostained with anti-Myc-tag and secondary anti-Alexa Fluor 488 green) in H1299 cells. Nucleus was stained with DAPI (*blue*); figures are shown with a *scale bar* of 20 μm. *C*, dimeric and tetrameric peaks of PKM, resolved by examining pyruvate kinase activity from the fractions collected after glycerol density gradient ultracentrifugation, loaded with protein lysates from H1299 cells. *D*, immunoblotting with anti-PKM1 and anti-PKM2 of the glycerol density gradient fractions as mentioned in *C* to measure the distribution of PKM1 and PKM2 in the separated peaks in *C*.

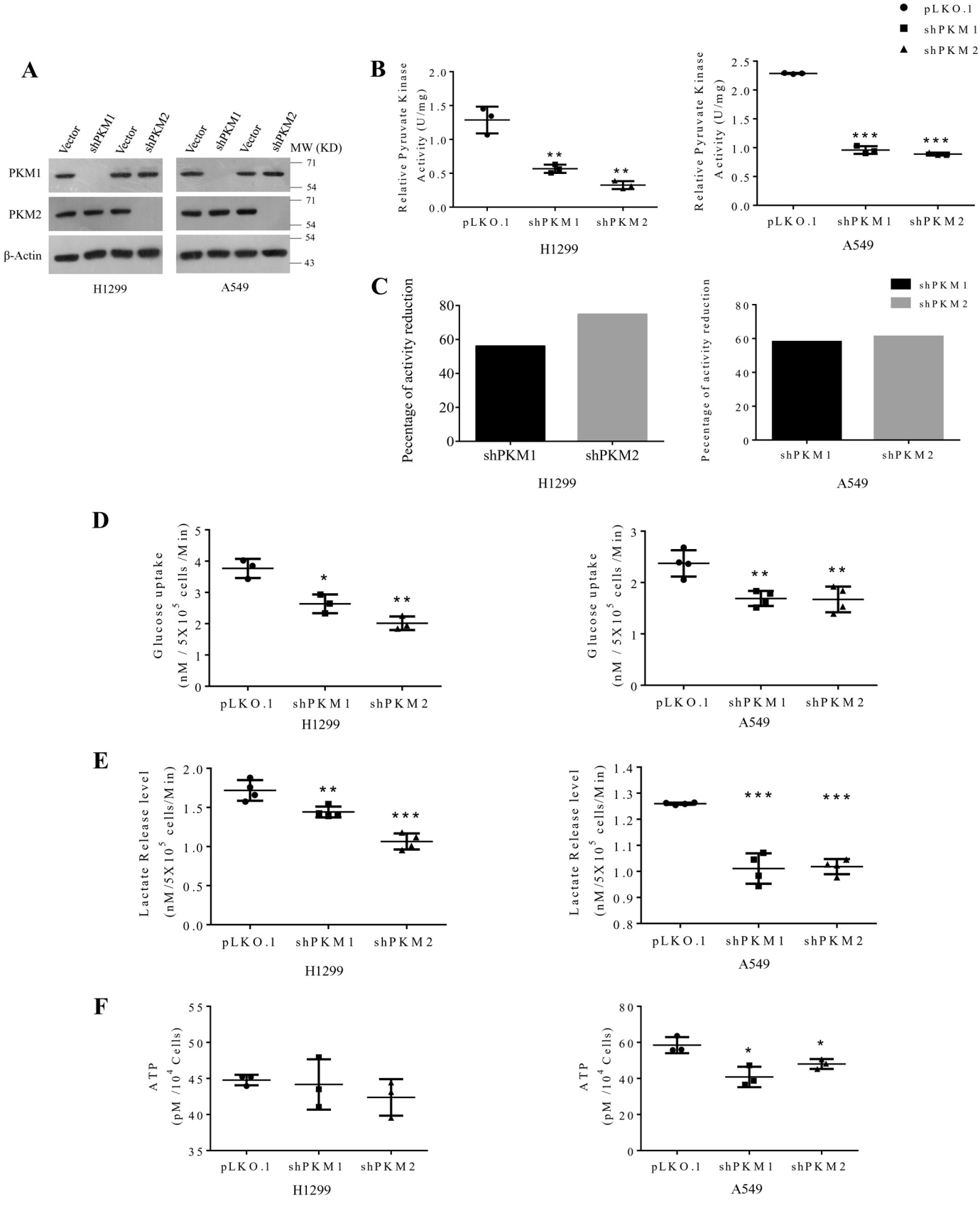
A
Vector
shPKM1
Vector
shPKM2
Vector
shPKM1
Vector
shPKM2
MW (KD)
PKM1
PKM2
β-Actin
71
54
71
54
54
43
H1299
A549
B
pLKO.1
shPKM1
shPKM2
Relative Pyruvate Kinase Activity (U/mg)
H1299
A549
C
Pecentage of activity reduction
shPKM1
shPKM2
H1299
A549
D
Glucose uptake (nM / 5X10^5 cells /Min)
H1299
A549
E
Lactate Release level (nM/5X10^5 cells/Min)
H1299
A549
F
ATP (pM /10^4 Cells)
H1299
A549

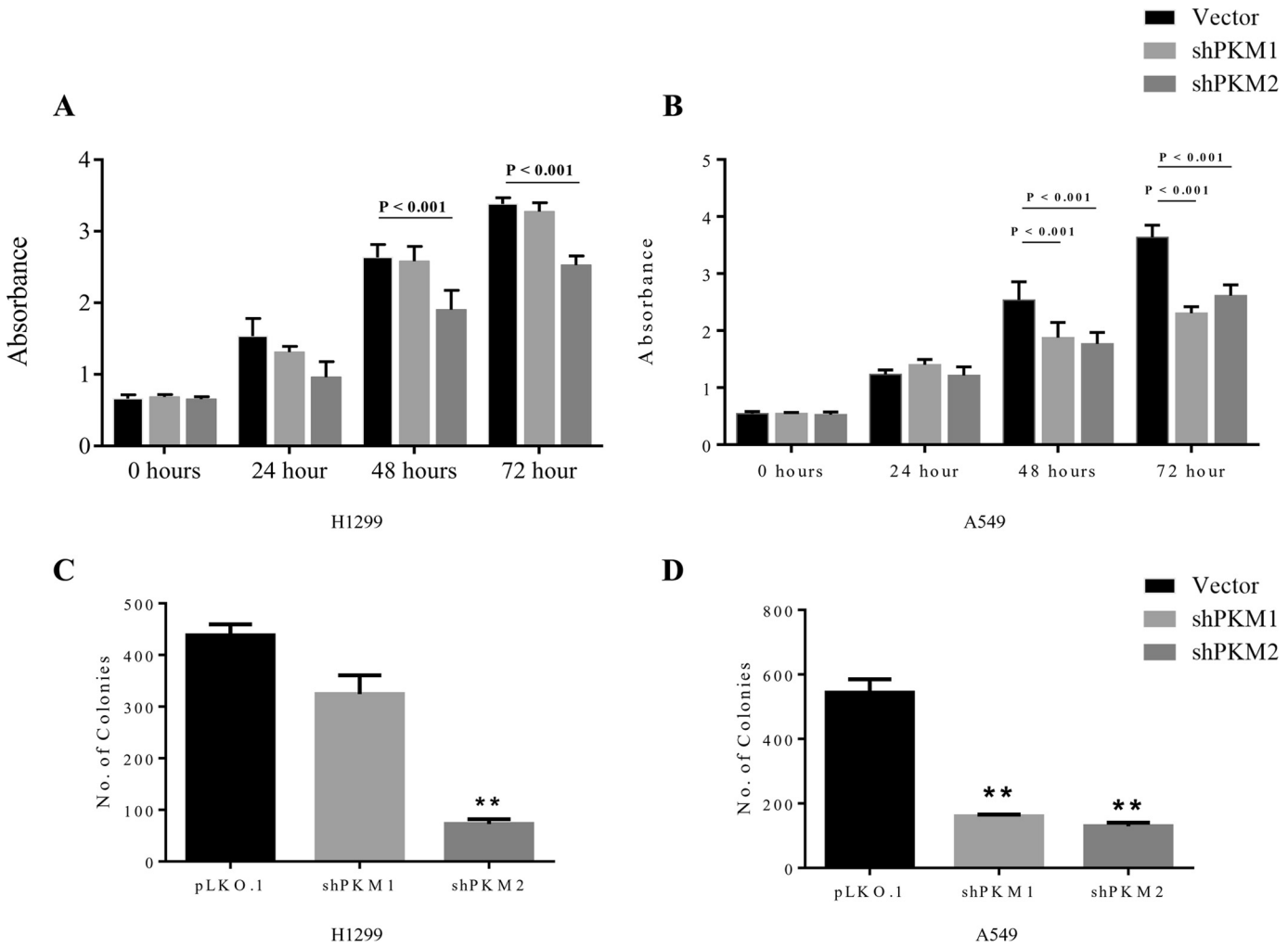

Figure 6. PKM1 or PKM2 silencing differentially affects the viability of H1299 and A549 (human lung cancer cells). *A* and *B*, CCK8 assay to examine the viability of H1299 cells (*A*) and A549 cells (*B*), transduced with vector (pLKO.1), shPKM1, or shPKM2 and cultured for the period of 72 h, the cellular viability assayed for every 24 h; with statistical analysis (where $n \geq 3$; mean ± S.D.), and the level of significance was tested using two-way analysis of variance with Tukey's multiple comparisons test. *C* and *D*, *bars* represent the number of colonies obtained from the anchorage-dependent clonogenic assay of H1299 (*C*) and A549 (*D*) stable cells transduced with lentivirus containing empty vector (pLKO.1), shPKM1, or shPKM2; with statistical analysis (where $n \geq 3$; mean ± S.D.), and the level of significance was tested using unpaired Student's *t* test.*, $p < 0.01$.

cells that were subjected to PKM2 knockdown exhibited 70% reduction in the net PK activity, whereas PKM1 knockdown reduced the activity by 55% in comparison to vector (pLKO.1) transfected cells (Fig. 5, *B* and *C*, *left panels*). In A549 cells silenced for PKM2, the activity was reduced by 61%, and PKM1 silencing reduced the activity by 58% (Fig. 5, *B* and *C*, *right panels*), suggesting a differential contribution of PKM2 and PKM1 isoforms to the net PK activity in the two (H1299 and A549) cell lines. Moreover, knockdown of either PKM1 or PKM2 contributed equally to reduce the glucose uptake and lactate release in these lung cancer cell lines (Fig. 5, *D* and *E*), the potential reasons for which are discussed later.

Intriguingly, stable knockdown of PK isoforms in A549 cells significantly reduced the cellular ATP level, whereas in H1299 cells the knockdown left the level of ATP unaltered (Fig. 5*F*). However, H1299 cells that were transiently transduced with shPKM1 or shPKM2 showed a reduction in the total cellular ATP level (data not shown), which probably suggests that H1299 stable cells for PKM1 and PKM2 knockdown that were passaged for successive generations attained energy homeostasis. When assayed for cellular viability, H1299 cells stably transduced with shPKM2 demonstrated a significant reduction in their viability (vector *versus* shPKM2, 48 h, $p < 0.001$ and 72 h, $p < 0.001$), whereas the cells transduced with shPKM1

Figure 5. Knockdown of PKM1 or PKM2 differentially affects the metabolism of human lung cancer cells H1299 and A549. *A*, immunoblots to validate the stable knockdown of PKM1 and PKM2 expression in H1299 (*left panel*) and A549 (*right panel*) cells, transduced with vector control (pLKO.1), shPKM1, or shPKM2. *B*, relative pyruvate kinase enzyme activity from protein lysates of H1299 (*left panel*) and A549 (*right panel*) cells stably transduced with control vector (pLKO.1), shPKM1, or shPKM2; with statistical analysis (where $n \geq 3$; mean ± S.D.), and the level of significance was tested using unpaired Student's *t* test. **, $p < 0.01$; ***, $p < 0.001$. *C*, bar diagrams showing a relative reduction in the percentage of pyruvate kinase activity after silencing of PKM1 and PKM2 in H1299 (*left panel*) and A549 (*right panel*) cells. *D–F*, glucose uptake (*D*), lactate release (*E*), and intracellular ATP (*F*) levels in H1299 (*left panel*) and A549 (*right panel*) cells stably transduced with vector (pLKO.1), shPKM1, or shPKM2; with statistical analysis (where $n \geq 3$; mean ± S.D.) and the level of significance was tested using unpaired Student's *t* test. *, $p < 0.05$; **, $p < 0.01$; ***, $p < 0.001$.

remained unaffected (Fig. 6*A*). Likewise, stable PKM2 knockdown in A549 cells showed a remarkable reduction in their viability (vector *versus* shPKM2, 48 h, $p < 0.001$ and 72 h, $p < 0.001$). However, in contrast to H1299, stable PKM1 knockdown in A549 cells also exhibited reduced viability (vector *versus* shPKM1, 48 h, $p < 0.001$ and 72 h, $p < 0.001$) (Fig. 6*B*). The effect of PKM silencing on H1299 and A549 cell viability was further validated using colony-forming assay, in which PKM2 silencing significantly affected H1299 propagation and colony formation (vector *versus* shPKM2, $p < 0.001$) (Fig. 6*C*), whereas knockdown of either PKM1 or PKM2 largely reduced A549 cell colony-forming ability (vector *versus* shPKM1, $p < 0.001$ and vector *versus* shPKM2, $p < 0.001$) (Fig. 6*D*).

PKM knockdown activates AMPK signaling to promote mitochondrial biogenesis and autophagy to evade apoptosis

The stable knockdown of PKM1 or PKM2 in H1299 cells activated the AMPK signaling pathway in response to the perturbed energy (ATP) homeostasis. The activation of AMPK was measured by a marked increase in threonine 172 (Thr-172) phosphorylation of AMPK, serine 79 (Ser-79) phosphorylation of acetyl-CoA carboxylase (ACC, a downstream substrate of AMPK), and serine 792 (Ser-792) phosphorylation of Raptor (adaptor protein of mammalian target of rapamycin (mTOR) complex 1) (Fig. 7*A, left panel*). In addition, AMPK activity was also assessed using the suppression of mTOR activity by a marked decrease in threonine 389 phosphorylation of p70S6 kinase. Conversely, stable PKM isoform knockdowns in A549 cells failed to activate AMPK because of the lack of the upstream protein kinase LKB1 (28–30) (Fig. 7*A*, *right panel*). Further, we uncovered here that the active AMPK in stable H1299 cells stimulated mitochondrial biogenesis, where activation of AMPK in H1299 cell was associated with concomitant increase in mitochondrial membrane potential ($\Delta\Psi m$) (Fig. 7*B*) and mitochondrial mass (Fig. 7*C*), with an overall increase in the expression of master regulatory transcription factors of mitochondrial biogenesis (PGC 1α, NRF1, NRF2, and TFAM) and mitochondrial-encoded subunits of electron transport chain (ETC) complexes (COX 1, ND3, and ATP6) (Fig. 7*D*). A549 cells that were silenced for the expression of PKM1 or PKM2 failed to show such changes in the mitochondrial membrane potential ($\Delta\Psi m$), mitochondrial content, and expression of genes associated with mitochondrial biogenesis (Fig. 7, *B* and *D*). Remarkably, H1299 cells that were silenced for PKM isoforms showed no sign of apoptosis but autophagy (Fig. 7*E*). This we established using LC3B Western blot analysis. The results revealed a significant increase in the LC3B-II band (Fig. 7*E*), an observation corroborated with the immunocytochemistry results, in which H1299 PKM1 and PKM2 knockdown stable cells when immunostained with LC3B antibody showed an increased autophagic punctate formation. The vector-transduced cells, however, showed a diffused pattern of LC3B immunostain (Fig. 7*F*). A549 cells that failed to activate AMPK pathway in response to PKM isoform silencing underwent apoptosis (depicted through poly(ADP-ribose) polymerase (PARP) cleavage using Western blot analysis), but not autophagy (Fig. 7*E*). Markedly, exogenous expression of constitutively active AMPKαT172D mutant rescued A549 cells silenced for PKM isoforms from apoptosis. Together, these results validated the significance of AMPK signaling in cancer cell survival following energy perturbation by the knockdown of PKM isoforms (Fig. 7*G*).

Knockdown of AMPKα catalytic subunits along with PKM1 or PKM2 induces apoptosis in H1299 cells

Given that PKM1 or PKM2 silencing in H1299 cells stimulated a metabolic shift to mitochondrial oxidative phosphorylation in an AMPK pathway–dependent manner to preserve energy homeostasis, we speculated that this reprogramming of energy metabolism might have warranted resistance against PKM1 and PKM2 silencing–induced cell death in H1299 cells. To test our hypothesis, we silenced the expression of AMPKα catalytic subunits in H1299 stable cells for PKM1 and PKM2 knockdown and validated with Western blot analysis (Fig. 8*A*). Further, we observed that the combination of AMPKα1/2 catalytic subunit and PKM1 or PKM2 knockdown in H1299 cells reduced the mitochondrial membrane potential ($\Delta\Psi m$) (Fig. 8*B*), mitochondrial mass (Fig. 8*C*), expression of genes associated with mitochondrial biogenesis (PGC 1α, NRF1, NRF2, and TFAM), and mitochondrial-encoded subunits of electron transport chain (ETC) complexes (COX 1, ND3, and ATP6) (Fig. 8*D*). When evaluated for cellular viability, H1299 cells that were transduced with the combination of shAMPKα and shPKM1 or shPKM2 demonstrated a significant reduction in their cellular viability (vector *versus* shAMPKα1/2 + shPKM1, 24 h, $p < 0.001$; 48 h, $p < 0.001$; and 72 h, $p < 0.001$) (vector *versus* shAMPKα1/2 + shPKM2, 24 h, $p < 0.001$; 48 h, $p < 0.001$; and 72 h, $p < 0.001$) (Fig. 8*E*) and also exhibited apoptotic cell death (Fig. 8*F*), Likewise, autophagy triggered by PKM1 and PKM2 silencing were abrogated by the concurrent transduction of shAMPKα1/2 (Fig. 8*F*).

Discussion

Altered metabolism phenotype of cancer cells has gained enormous attention in recent years. Attempts have been made to develop drugs that could target important metabolic enzymes like PKM2, which arguably is the critical regulator of aerobic glycolysis in cancer cells. The therapeutic intervention that involves the strategy of silencing the expression of PKM2 has several limitations. Although the knockdown of PKM2 affects aerobic glycolysis in cancer cells (4), its ability in regressing the proliferation and in inducing cell death of cancer cells from distinct tissue origin has been debated (20–22, 26, 27, 32).

Our experiments in a representative set of human cancer cell lines of different tissue origin have showed co-expression of M1 and M2 isoforms of pyruvate kinase (Fig. 1), except for HeLa cells. The HeLa cells showed a strong presence of PKM2 and PKM1 isoforms at RNA level and exhibited a relatively low expression of PKM1 because of a partial proteolytic degradation of PKM1[3] along with high expression of PKM2 at protein level.

The observation of co-expression of the two isoforms in both cancer cell lines and tumor samples provided us an insight to

[3] G. Prakasam, R. K. Singh, M. A. Iqbal, S. K. Saini, A. B. Tiku, and R. N. K. Bamezai, unpublished results.

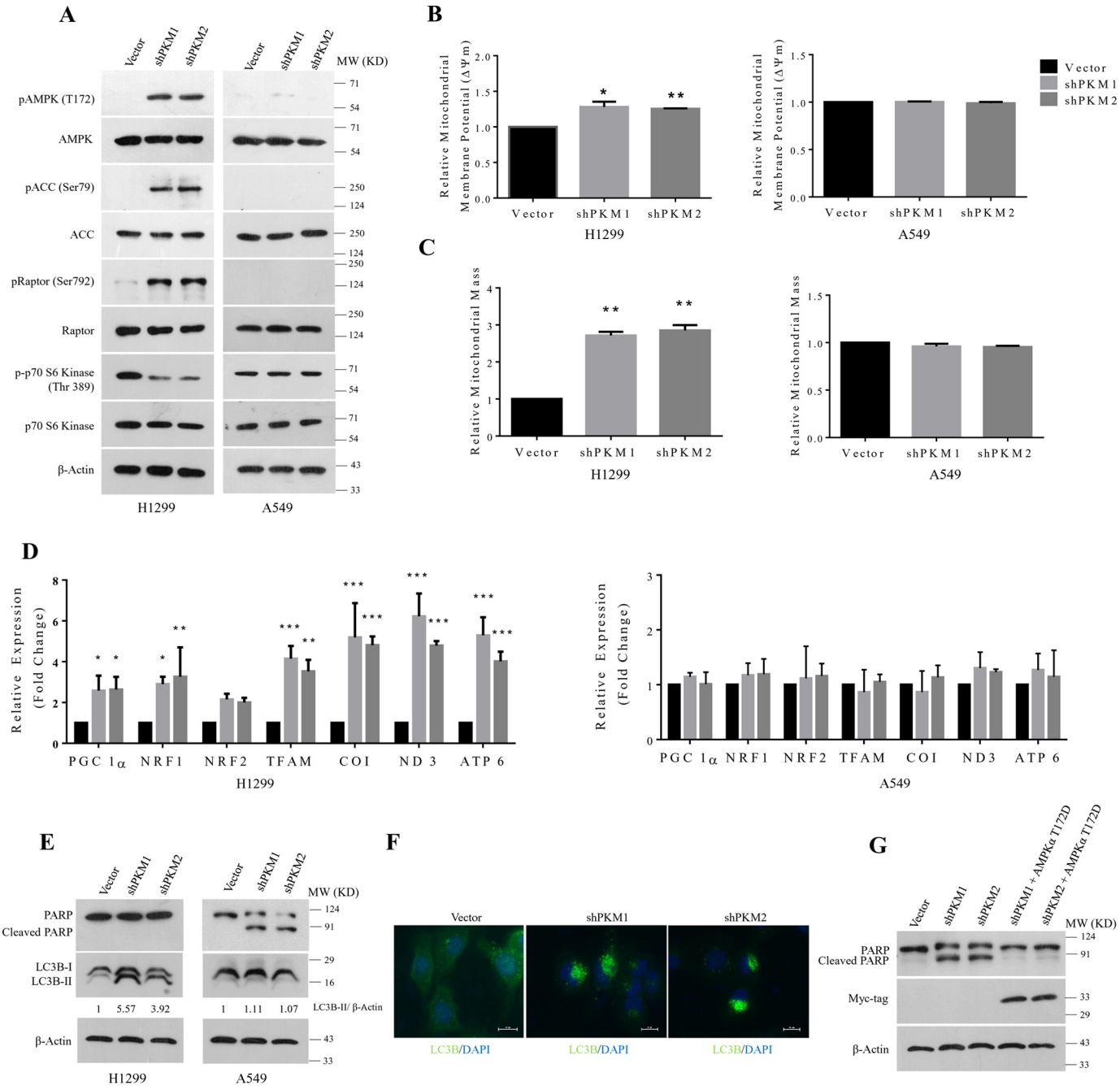

Figure 7. AMPK signaling reprograms energy metabolism pathway to sustain energy homeostasis and to prevent apoptotic cell death. *A*, immunoblots from the protein lysate of H1299 (*left panel*) and A549 (*right panel*) cells stably transduced with lentivirus containing control vector (pLKO.1), shPKM1, or shPKM2, to show AMPK signaling activation. *B* and *C*, bar diagram depicts the relative mitochondrial membrane potential (*B*) and mitochondrial mass (*C*) in H1299 (*left panels*) and A549 (*right panels*) cells stably transduced with control vector (pLKO.1), shPKM1, or shPKM2; with statistical analysis (where $n \geq 3$; mean ± S.D.), and the level of significance was tested using unpaired Student's *t* test. *, $p < 0.05$; **, $p < 0.01$. *D*, quantitative RT-PCR analysis to show the relative expression change of genes involved in the mitochondrial biogenesis (PGC 1α, NRF1, NRF2, and TFAM) and mitochondrial-encoded subunits of electron transport chain complexes (COX 1, ND3, and ATP6) from H1299 (*left*) and A549 (*right*) cells for stable PKM1 and PKM2 knockdown. The *bars* represent the -fold change after normalizing with the control of each group (vector transfected); with statistical analysis (where $n \geq 3$; mean ± S.D.) and the level of significance was tested using two-way analysis of variance with Tukey's multiple comparisons test. *, $p < 0.05$; **, $p < 0.01$; ***, $p < 0.001$. *E*, immunoblots from the protein lysate of H1299 (*left panel*) and A549 (*right panel*) cells transduced with lentivirus containing empty vector (pLKO.1), shPKM1, or shPKM2 to measure autophagy and apoptosis using LC3B-II and cleaved PARP as markers. *F*, confocal microscopy images depicting the autophagic puncta formation in H1299 cells stably transduced with shPKM1 and shPKM2, immunostained with LC3B antibody and secondary anti-Alexa Fluor 488. Nucleus was stained with DAPI (*blue*). Merged figures are shown with a *scale bar* of 20 μm. *G*, immunoblot from the protein lysate of A549 cells, transduced with lentivirus containing empty vector (pLKO.1), shPKM1, shPKM2, and, in addition, ectopic expression of Myc-tagged AMPKα2 constitutively active T172D mutant (AMPKα2T172D-Myc) in cells knocked down for PKM1 and PKM2 probed with Myc-tag and PARP antibodies to validate the expression of AMPKα2T172D-Myc and to measure apoptosis.

suggest alternative approaches for therapeutic intervention in cancer cells. We propose that the cancer cells express both the isoforms of PKM which interact to generate heterotetrameric cross-oligomers (Figs. 2 and 4), besides homotetramers of PKM1, PKM2, and homodimers of PKM2, in all probability contributing to the overall pyruvate kinase activity in cancer

cells. Thus, it is obvious from our results that cancer cells involve both PKM1 and PKM2 to drive the glycolysis to yield ATP (Fig. 5), also indicating that PKM1 in cancer cells is not just a bystander.

Hence, we believe a stand-alone therapeutic strategy that silences the expression of PKM2 might not warrant success in regressing the tumor propagation. The abrogation of PKM2 expression in such a situation may be compensated by the

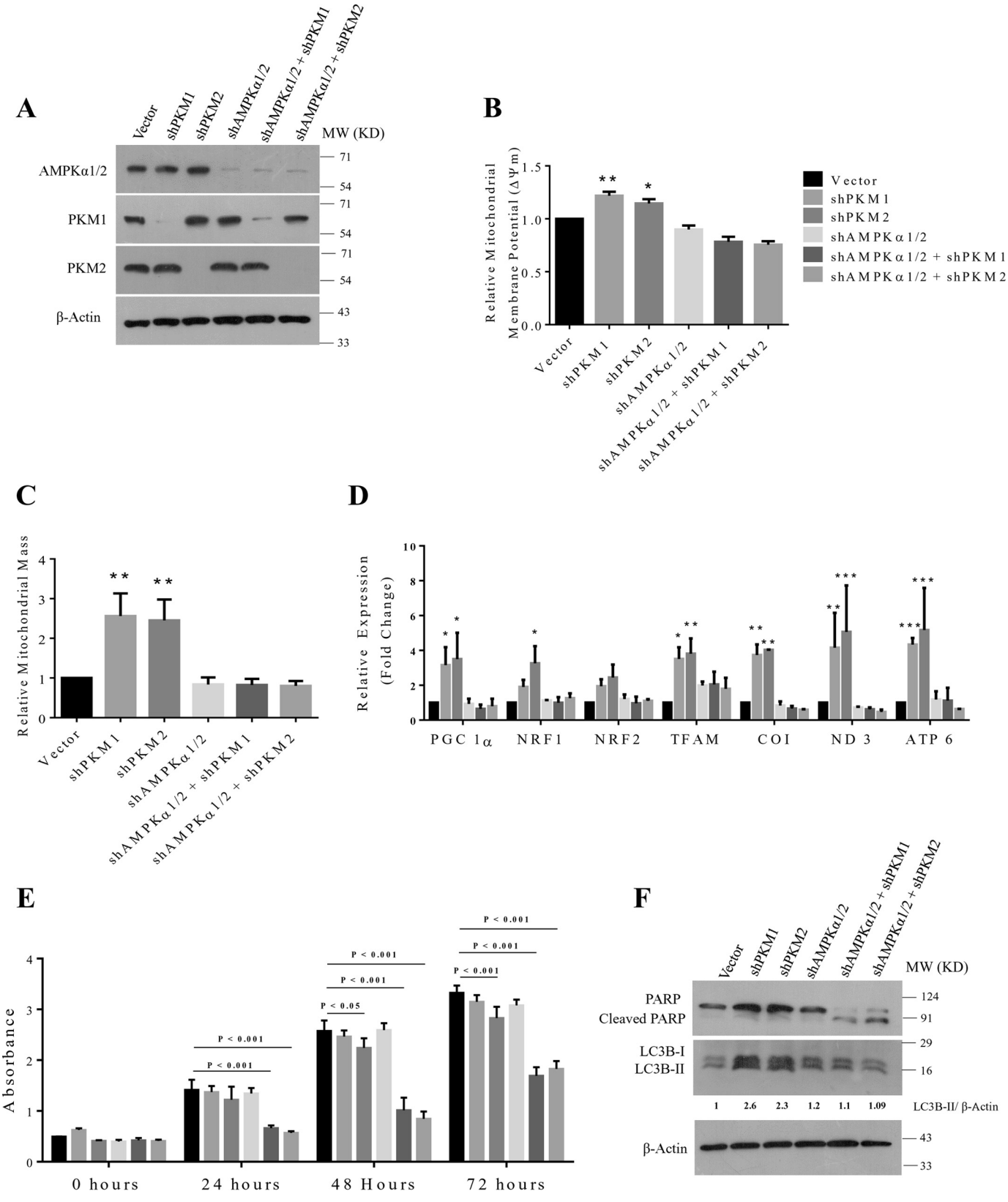

expression of PKM1 or the signaling pathway that reprograms energy metabolism to preserve energy homeostasis. This opinion is supported by a recent study conducted by Israelsen *et al.* (27), in which PKM2 knock out reprogrammed tumors to express PKM1, which instead of regressing, stimulated tumor propagation. A recent study by Qin *et al.* (32) states that Akt survival signaling that activated, followed by PKM2 knockdown, conferred protection against growth inhibition and apoptosis.

Interestingly, our data demonstrated that the knockdown of PKM1 and PKM2 affected pyruvate kinase activity, cellular ATP level, and viability of A549 and H1299 cells (lung adenocarcinoma cells) differentially (Figs. 5 and 6). Because the dimeric and tetrameric content of pyruvate kinase was different in H1299 and A549 cells (data not shown), it is expected that the overall PK activity in the two cell lines may differ. Also, the activity of an enzyme does not always correlate with the mRNA and protein content, because of post-translational modifications and existence of different oligomeric forms of an enzyme (allosteric regulation). PKM1 is a constitutively active and PKM2 an allosteric isoform with their tetramers expected to have substantial differences in the activity. Further, as a rule, constitutively active enzymes usually have higher activities compared with the allosteric isoforms (5, 8, 9). The analysis, however, of the H1299 and A549 cells knocked down for PKM1 or PKM2, did not show any difference between the two cell lines when studied for glucose uptake and lactate release level, and the results of reduction were more or less similar. We conjecture two potential reasons for this reduction: (i) the knockdown of PKM apparently allows accumulation of its substrate P-enolpyruvate (PEP) (26), allosterically inhibiting the rate-limiting glycolytic enzyme PFK1 through a feed-forward mechanism (33, 34), largely affecting the rate of glucose uptake and glycolytic flux by inhibiting PFK1 and (ii) the knockdown of PKM2 abrogates its transcriptional co-activation function with HIF1α in regulating the expression of enzymes, GLUT1 and LDHA, associated with glucose metabolism through a positive feedback loop (9, 14) and reducing the glucose uptake.

Later, we also uncovered that the heterogenic response between PKM-silenced H1299 and A549 cells was because of the presence of LKB1 (a serine/threonine protein kinase upstream to AMPK) and an active AMPK signaling network downstream to LKB1 in H1299 and its absence in A549 cells (28–30) (Fig. 7*A*). H1299 cells that were silenced for PKM isoforms, to evade apoptosis, activated AMPK survival signaling to reprogram energy metabolism (Fig. 9*A*) by stimulating mitochondrial biogenesis and by triggering autophagy, confirmed in Western blot analysis and by the formation of autophagic puncta in immunocytochemical studies, to preserve energy homeostasis (Fig. 7). A549 cells that lack LKB1, however, failed to activate AMPK to maintain the adaptive energy metabolic phenotype governed by AMPK, resulting in enhanced growth inhibition and apoptosis (Figs. 6 and 7). The ectopic expression of constitutively active AMPK mutant (AMPK T172D) in A549 cells, which did not require LKB1 presence for its activation, rescued PKM knockdown–induced cell death (Fig. 7*G*); confirming the role of AMPK in cell survival.

Our observation of induction of autophagy in H1299 stable cells for PKM1 and PKM2 knockdown is consistent with a recent study by Zhang *et al.* (35), wherein it was shown that AMPK regulated the expression of key autophagic marker ULK1 and LC3B in a FoxO3 (transcription factor)– dependent manner. It is well-known that AMPK directly stimulates autophagy by phosphorylating Ulk1 at Ser-317 and Ser-777 residues (36). Because AMPK was activated upon PKM silencing in our case, it may explain our results in which LC3B-II is increased without any decrease in LC3B-I. Notably, the requirement of AMPK in both up-regulation of LC3B and conversion of LC3B-I to LC3B-II was observed by us as shown in Fig. 8*F*.

The importance of this study in the context of lack of LKB function affecting the AMPK signaling path becomes obvious from the fact that nearly 20–30% of lung adenocarcinomas are known to either lack LKB1 or harbor a loss of functional mutation (37). In addition, a substantial number of cases with cervical, endometrial, and prostate cancers also carry LKB1 mutations (38). Loss of LKB1 expression has been linked largely to a deregulated cellular metabolism, which generally relies on aerobic glycolysis and supports the aggressive replicative phenotype of the tumors by delivering precursors for biosynthesis (28, 39, 40). Taken together, our results suggest that the cancer cells with aberrant LKB1-AMPK axis could be contained by targeting glycolytic metabolism and energy homeostasis through PKM1 and PKM2 silencing (Figs. 7 and 9, *B* and *C*). We find our conclusions are consistent with recent studies, which collectively demonstrate that triggering bioenergetic stress by pharmacological or genetic means in LKB1-AMPK pathway–deficient tumors could enhance anti-tumorigenic effect (29, 41–43).

Our study also demonstrates that the cancer cells with active LKB1 could be targeted by employing a strategy of introducing a combination of knockdowns for AMPKα catalytic subunits and PKM1 or PKM2 (Figs. 8 and 9, *D* and *F*). To this end, we find targeting AMPK could be appealing over LKB1, because LKB1

Figure 8. AMPKα2 and PKM1 or PKM2 dual knockdown induces cell death in H1299 cells by preventing energy metabolism reprogramming. *A*, immunoblots from the protein lysate of H1299 cells stably transduced with control vector (pLKO. 1), shPKM1, shPKM2, shAMPKα1/2, and shAMPKα1/2 + shPKM1 or + shPKM2 to validate the knockdown of AMPKα1/2, PKM1, and PKM2. *B* and *C*, bar diagram depicts the relative mitochondrial membrane potential (*B*) and mitochondrial mass (*C*) in H1299 cells stably transduced with control vector (pLKO.1), shPKM1, shPKM2, shAMPKα1/2, and shAMPKα1/2 + shPKM1 or + shPKM2; with statistical analysis (where $n \geq 3$; mean ± S.D.), and the level of significance was tested using unpaired Student's *t* test. *, $p < 0.05$, **, $p < 0.01$. *D*, quantitative RT-PCR analysis to show the relative expression change of genes involved in the mitochondrial biogenesis (PGC 1α, NRF1, NRF2, and TFAM) and mitochondrial-encoded subunits of electron transport chain complexes (COX 1, ND3, and ATP6) from H1299 cells for stable shPKM1, shPKM2, AMPKα1/2, or AMPKα1/2 and PKM1 or PKM2 knockdown. The *bars* represent the -fold change after normalizing with the control of each group (vector transfected); with statistical analysis (where $n \geq 3$; mean ± S.D.), and the level of significance was tested using two-way analysis of variance with Tukey's multiple comparisons test. *, $p < 0.05$; **, $p < 0.01$; ***, $p < 0.001$. *E*, CCK8 assay to examine the viability rate of H1299 cells stably transduced with control vector (pLKO.1), shPKM1, shPKM2, shAMPKα1/2, and shAMPKα1/2 and shPKM1 or shPKM2 and cultured for the period of 72 h. Cellular viability rates were assayed for every 24 h; with statistical analysis (where $n \geq 3$; mean ± S.D.), and the level of significance was tested using two-way analysis of variance with Tukey's multiple comparisons test. *F*, immunoblots from the protein lysate of H1299 as mentioned in (*A*) to measure autophagy and apoptosis using LC3B-II and cleaved PARP as markers.

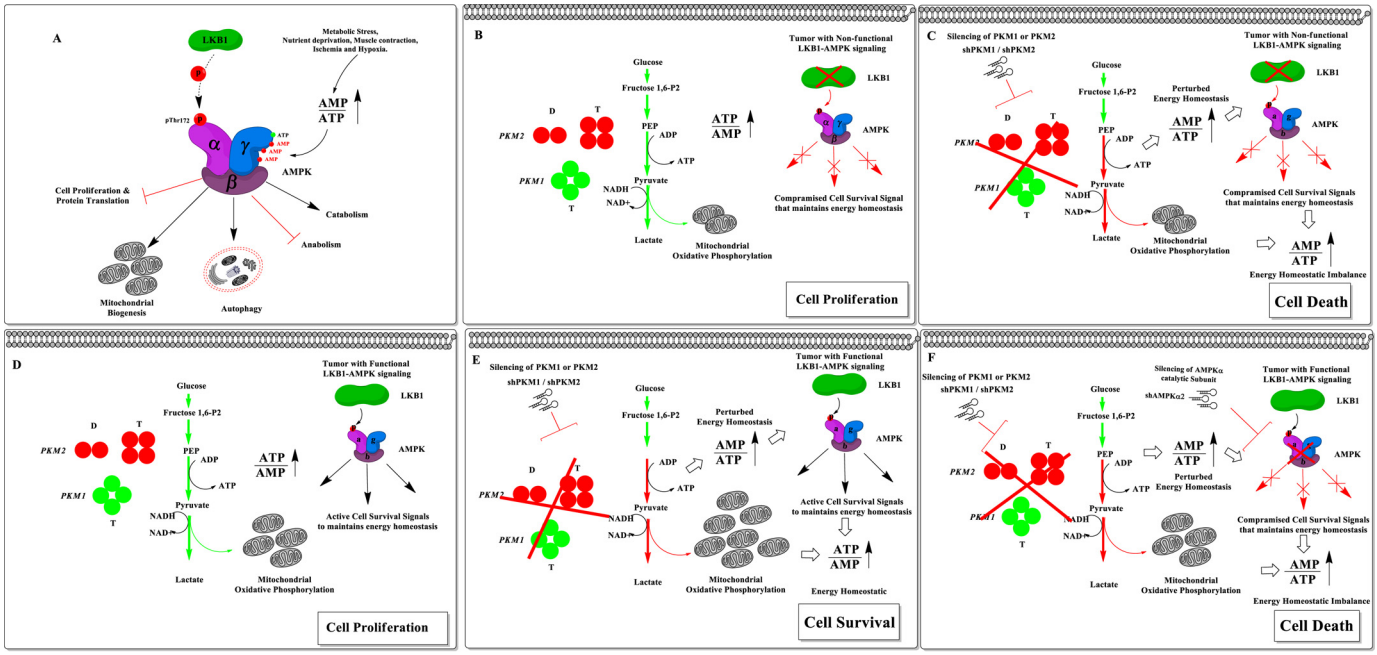

Figure 9. Schematic representation of the proposed therapeutic strategy to improve the efficacy of PKM targeting therapy in cancer cells in the background of the cellular status of the LKB1-AMPK pathway. *A*, the effect of the bioenergetic sensor, LKB1-AMPK signaling on cellular metabolic pathways to preserve energy homeostasis. *B*, the pro-growth metabolic phenotype of tumor cells that lacks or expresses a nonfunctional LKB1 (*i.e.* somatic mutation, promoter hypermethylation, or exonic deletion) and thus fails to activate the bio-energetic sensor AMPK. *C*, the therapeutic efficacy of PKM2 or PKM1 silencing in tumor cells that lack LKB1-AMPK signaling pathway to rewire metabolic phenotype and to restore the perturbed ATP level. *D*, the metabolic phenotype of tumor cells that possess the intact bio-energetic sensors, LKB1-AMPK signaling pathway. *E*, the mechanistic insight of LKB1-AMPK mediated metabolic rewiring and the restored energy homeostasis that confers treatment resistance against PKM silencing in cancer cells. *F*, the proposed therapeutic scheme of inducing synthetic lethality in cancer cells by targeting the pro-growth metabolism by silencing PKM isoforms and reducing resistance toward apoptosis by targeting the AMPK pathway.

confers most of its biological role of cellular energy metabolic reprogramming of the bioenergetic sensor AMPK via phosphorylation of Thr-172 residue of AMPK (44, 45). Numerous strategies that choose to target aerobic glycolysis are underway; our study here emphasizes that the cancer cells could develop resistance against those strategies through AMPK-dependent energy metabolic rewiring. Taken together, our findings provide a rationale for PKM knockdown in LKB1-deficient lung cancer cells and in addition, proposes that the combined silencing of AMPK and PKM isoforms through genetic or pharmacological means may provide a promising therapeutic strategy that could curtail the tumor cells with a functional LKB1-AMPK axis (Fig. 9).

Experimental procedures

Cell culture and tumor tissue samples

Cell lines MCF-7 (human breast adenocarcinoma), MDA-MB-231 (human breast adenocarcinoma), PC-3 (human prostate adenocarcinoma), H1299 (non–small cell lung carcinoma), A549 (lung carcinoma), HeLa (human cervical adenocarcinoma), HEK293T (human embryonic kidney cell line), and L6 (rat skeletal muscle), procured from the American Type Culture Collection (ATCC) or National Centre for Cell Science (NCCS, Pune, India), were grown in DMEM (Sigma-Aldrich), supplemented with 1× penicillin/streptomycin from 100× stock solution (Sigma-Aldrich), 10% fetal bovine serum (FBS) (Gibco), and maintained in the incubator (Thermo Scientific Heraeus) at 37 °C with 5% CO_2. Tumor tissues from sporadic breast cancer patients (provided by Dr. Gaurav Agarwal from Sanjay Gandhi Postgraduate Institute of Medical Sciences, Lucknow, India) were collected as detailed earlier (46, 47) with the prior approval from Jawaharlal Nehru University Institutional Ethics Committee.

Cloning and site-directed mutagenesis

The coding sequences (CDs) of full-length PKM1 and the truncated AMPKα2 were amplified by PCR from cDNA of H1299 cells. In brief, the insertion of M1 isoform of *PKM* gene was generated by an overlapping PCR using the PKM1/2 CDs–specific and Exon 9–specific primers. PKM1/2 (forward 5′-ATATGAATTCATGTCGAAGCCCCATAGTGAAG-3′ and reverse 5′-ATATGGATCCCGGCACAGGAACAACACGCA-3′), PKM Exon 9 (forward 5′-AGGCAGCCATGTTCCAC-3′ and reverse 5′-TGCCAGACTCCGTCAGAACT-3′), AMPKα2 (forward 5′-ATATGGATCCATGGCTGAGAAGCAGAAGCA-3′), and AMPKα2 312 (reverse 5′-ATATAAGCTTATATAAACTGTTCATTACTTCTGATTCTGT-3′). The PCR-amplified fragment was sequenced and cross-checked for background mutations and cloned in pcDNA^{TM}3.1/myc-His(−)A vector. Expression vector pcDNA^{TM}3.1/myc-His(−) A, lentiviral transfer vector (pLKO.1), and packaging vectors (psPAX and pMD2.G) were a kind gift from Prof. Shyamal K Goswami and Dr. Goutam K Tanti (School of Life Science, Jawaharlal Nehru University, New Delhi). Lentiviral transducing vector, pLKO.1 encoding shPKM1, and shPKM2 were a generous gift from Dr. Marta Cortés-Cros (Novartis, Basel, Switzerland). Lentiviral shRNA vectors targeting the expression AMPKα1 and AMPKα2 (catalog no. pLKO.1shAMPKα1-

TRCN0000000861 and pLKO.1shAMPKα2-TRCN0000002171) were procured from Sigma-Aldrich. Site-directed mutagenesis was performed using QuikChange Site-Directed Mutagenesis Kit (Agilent Technologies), according to the manufacturer's protocol. In brief, wild-type (WT) construct of AMPKα2 was truncated to delete the autoinhibitory and β,γ subunit-binding domain and used for generating AMPKα2 constitutively active T172D mutant by site-directed mutagenesis (AMPKα2T172D forward 5′-TTTCTGAGAGATAGTTGCGGA-3′ and AMPKα2T172D 5′-reverse TCCGCAACTATCTCTCAGAAA-3′). The PCR-amplified fragment was sequenced and cross-checked for site-directed mutations incorporated and cloned in pcDNA^{TM}3.1/myc-His(−) A vector.

Generation of stable gene expressing, and knockdown cell lines

To establish stable gene expression, the pcDNA-PKM1-Myc construct was transfected using Lipofectamine® 3000 reagent (Thermo Fisher Scientific) as per the manufacturer's instructions. Briefly, after 48 h of post transfection, cells were selected in G418 (1 mg/ml) containing selection medium for 2 weeks to generate stable cell lines. For stable gene knockdowns, the lentiviral particles were generated as described previously (26, 31, 48). In brief, HEK293T cells were transfected with transfer vector (LKO.1) harboring shRNAs, along with packaging vectors, psPAX, and pMD2.G, using Lipofectamine® 3000 reagent (Thermo Fisher Scientific). After 48 h of post transfection, viral particles were harvested (in polypropylene microfuge tubes), concentrated, and used to infect/transduce the target cells in presence of hexadimethrine bromide (Polybrene). Infected cells were selected in puromycin (2 μg/ml) containing DMEM for the course of 14 days for generating cell lines with stable gene knockdown.

Immunoblotting

Immunoblot analysis was performed by lysing the cells in modified RIPA buffer (50 mM Tris-HCl pH 7.2, 150 mM NaCl, 0.5% sodium deoxycholate, 0.1% SDS, 1% Triton X-100) supplemented with 1 mM PMSF, protease inhibitor mixture and phosphatase inhibitor mixture II and III (Sigma-Aldrich). Protein lysates were cleared by centrifugation and concentrations quantified using a BCA kit (Thermo Scientific). An equal amount of protein lysate was resolved in SDS-PAGE, transferred to nitrocellulose membrane, and probed with primary antibodies of interest. Protein bands were detected using Luminata Forte (EMD Millipore). Densitometry analysis was performed using ImageJ software to calculate the relative expression change after normalizing with β-actin. Primary antibodies used in the study were as follows: PKM1 (catalog no. SAB4200094), PKM2 (catalog no. SAB4200095), Myc-tag (catalog no. C3956), LC3B (catalog no. L7543), and β-actin (catalog no. A1978) were procured from Sigma-Aldrich, and AMPKα (catalog no. 5831), phospho-AMPKα (Thr-172) (catalog no. 2535), acetyl-CoA carboxylase (catalog no. 3676), phospho-acetyl-CoA carboxylase (Ser-79) (catalog no. 11818), PARP (catalog no. 9542), Raptor (catalog no. 2280), phospho-Raptor (Ser-792) (catalog no. 2083), p70 S6 kinase (catalog no. 2708), p70 S6 kinase kit (catalog no. 9234), β-tubulin (catalog no. 2128), and histone H3 (catalog no. 4499) were obtained from Cell Signaling Technology. Secondary antibodies, anti-mouse HRP (catalog no. 7076), and anti-rabbit HRP (catalog no. 7074) were from Cell Signaling Technology.

Subcellular fractionation and co-immunoprecipitation

Nuclear and cytoplasmic fractions were obtained by using the NE-PER extraction kit (Thermo Scientific) and fractions of mitochondria were extracted using mitochondrial isolation kit (Thermo Scientific), according to the manufacturer's instructions. Co-immunoprecipitation was performed using the kit procured from Thermo Scientific. In brief, the antibodies were cross-linked with the amine-activated agarose A beads and incubated with cell lysates at 4 °C overnight. Protein complexes bound to the beads were washed three times with lysis buffer and then eluted by adding elution buffer. The resultant immunoprecipitation products and inputs were subjected to immunoblotting analysis with the antibodies of interest.

Confocal microscopy

Cells grown on coverslips were fixed by adding 3.7% paraformaldehyde, dissolved in phosphate-buffered saline (PBS) for 20 min and cells were permeabilized with blocking buffer (5% chicken serum in 1X PBS) containing 0.1% Triton X-100 for 1 h at room temperature. Slides were incubated overnight at 4 °C with primary antibodies to mark their subcellular localization. Excessive antibodies were washed and incubated with secondary antibodies, anti-rabbit Alexa Fluor 488 or anti-rabbit Alexa Fluor 594 or anti-mouse Alexa Fluor 488 (Thermo Fisher Scientific) for 1 h at room temperature. Nuclei were stained with DAPI (Sigma-Aldrich) and the mitochondria were stained with MitoTracker Red (Molecular Probes, Life Technologies). Coverslips were mounted on glass slides with Prolong® AntiFade Reagent (Molecular Probes, Life Technologies); cells were examined and an image obtained using Nikon Eclipse Ti-S Inverted Microscope. The data were analyzed using NIS-Elements Imaging Software (Nikon).

RT-PCR

Total RNA isolated from cells with TRI Reagent (Sigma-Aldrich) was reverse transcribed into cDNA, using SuperScript^{TM} III Reverse Transcriptase kit (Life Technologies). Quantitative RT-PCR analysis was carried out in Bio-Rad CFX96 Touch^{TM} Real-Time PCR Detection System, using SYBR Green PCR Master Mixture (Applied Biosystems). The relative gene expression was calculated using the comparative *Ct* method ($2^{-\Delta\Delta Ct}$). Results were analyzed and presented as -fold change after normalizing with the control group. Actin served as an endogenous control. Primers used for the RT-PCR analysis are as follows: PGC1 A (forward 5′-TGTCACCACCCAAATCCTTATTT-3′ and reverse 5′-TGTGTCGAGAAAAGGACCTTGA-3′), NRF1 (forward 5′-CCATCTGGTGGCCTGAAG-3′ and reverse 5′-GTGCCTGGGTCCATGAAA-3′), NRF2 (forward 5′-ACACGGTCCACAGCTCATC-3′ and reverse 5′-TGTCAATCAAATCCATGTCCTG-3′), TFAM (forward 5′-GAACAACTACCCATATTTAAAGCTCA-3′ and reverse 5′-GAATCAGGAAGTTCCCTCCA-3′), COI (forward 5′-TTCTGACTCTTACCTCCCTCTC-3′ and reverse 5′-TGGGAGT-

AGTTCCCTGCTAA-3′), ND3 (forward 5′-CCACAACTCA-ACGGCTACATA-3′ and reverse 5′-AGGAGGGCAATTTC-TAGATCAAA-3′), ATP6 (forward 5′-TAGCCCACTTCTTA-CCACAAGGCA-3′ and reverse 5′-TGAGTAGGTGGCCTG-CAGTAATGT-3′), and ACTIN (forward 5′-ACTCTTCCAG-CCTTCCTTC-3′ and reverse 5′-ATCTCCTTCTGCA-TCCTGTC-3′).

Semi-quantitative RT-PCR assay to examine PKM1/PKM2 mRNA proportion

RNA was isolated from 2×10^6 cells using TRI Reagent (Sigma-Aldrich). 2 μg from total RNA was subjected to DNase I (Applied Biosystems) treatment to remove contaminating DNA and was reverse transcribed into cDNA using SuperScript™ III Reverse Transcriptase kit (Life Technologies). PKM alternative splice transcripts, PKM1 (Exon 9 included) and PKM2 (Exon 10 included), were PCR amplified together using primers specific to Exon 8 and Exon 11 (Exon-8 5′-GAAACAGCCAAAGGGGACT-3′ and Exon-11 5′-CATT-CATGGCAAAGTTCACC-3′) as described earlier (7). The amplified products were equally divided into two aliquots (~ 20 μl); one of them was subjected to restriction digestion with Ale I restriction enzyme and the other one served as an uncut control. Ale I specifically cuts at Exon 10 of PKM2 and leaves PKM1 undigested. Images of semi-quantitative RT-PCR products resolved in 3% agarose gel were obtained by Syngene gel documentation system.

LC-MS studies

His- and Myc-tagged PKM1 was purified from the lysates of H1299 stable cells using His pulldown and Myc IP. We first used His-tag for pulldown and then immunoprecipitated PKM1 using Myc-tag from the elute we got after His pulldown. The resultant eluent was subjected to in-solution trypsin digestion. In brief, the eluted proteins were mixed with surfactant RapiGest (Waters) and were reduced with DTT and alkylated using iodoacetamide. Samples were digested with 2 μg of sequencing grade trypsin gold (Promega) at 37 °C overnight and subjected to LC-MS-MS analysis (LC-MS-MS Waters SYNAPT G2 with 2D nano ACQUITY System). Mass spectrum obtained from the LC-MS was analyzed using ProteinLynx Global SERVER and the interactome for PKM1 was generated.

Computational prediction of protein subcellular localization

To predict subcellular localization of PKM1 (UniProt I.D.: P14618–2) and PKM2 (UniProt I.D.: P14618–1), the amino acid sequences of PKM isoforms were examined using six online computation tools that employ various algorithms to predict the subcellular localization. In brief, these tools employ algorithms that involve homology-based annotation, amino acid composition, localization signal sequences (sorting signals), and functional motifs to predict the subcellular localization. We used the following computational tools to assess the subcellular localization of PKM isoforms: CELLO v.2.5, http://cello.life.nctu.edu.tw/ (50, 51); HSLpred, http://www.imtech.res.in/raghava/hslpred/ (52); Hum-mPLoc 2.0, http://www.csbio.sjtu.edu.cn/bioinf/hum-multi-2/ (53, 54); SubLoc v1.0, https://omictools.com/subloc-tool (55); YLoc, http://abi.inf.uni-tuebingen.de/Services/YLoc/webloc.cgi (56, 57); and BaCelLo, http://gpcr.biocomp.unibo.it/bacello/ (58).[4]

Pyruvate kinase enzyme assay and glycerol gradient ultracentrifugation

Pyruvate kinase activity was measured as described previously (10). In brief, PK catalytic activity was measured by coupling with lactate dehydrogenase assay.

The specific activity of enzymes per mg of cell lysate was calculated as follows.

$$\text{Units mg} = \frac{\text{OD}_{340}/\text{min}}{6.22 \times \text{mg lysate/ml reaction}} \quad \text{(Eq. 1)}$$

Glycerol gradient ultracentrifugation experiment was performed by loading 750 μg of whole cell protein lysate on top of 15–33% step gradient and centrifuged at 50,000 rpm for 18 h at 4 °C in a SW 55 Ti Rotor (Beckman Coulter); fractions were collected and examined for PK activity as mentioned previously (12). An aliquot of these fractions was subjected to immunoblot analysis.

Glucose uptake, lactate release, and ATP assays

Glucose consumption and lactate release levels were measured in culture medium that was collected after growing cells under appropriate conditions, using a glucose (hexokinase) assay kit (Sigma-Aldrich) and Lactate Colorimetric/Fluorometric Assay Kit (BioVision) following the manufacturer's specifications. The concentration of the ATP was measured using the ATP bioluminescence assay kit (BioVision) as per the manufacturer's instruction.

FACS analysis

To assess the mitochondrial membrane potential and mass, the stable knockdown cells were trypsinized and stained with 100 nM MitoTracker Red CMXROS dye (Invitrogen, catalog no. M7512) to examine mitochondrial membrane potential or MitoTracker Green dye (Invitrogen, catalog no. M7514) to examine mitochondrial mass and incubated for 30 min at 37 °C. To acquire the fluorescence MitoTracker signals, samples were run on flow cytometry (BD Biosciences), and the data acquired were analyzed using built-in CellQuest Pro Software.

Cell Counting Kit-8 (CCK8) assay to measure cell viability

The viability of cultured cells, transduced with shPKM1 and shPKM2 were measured using Cell Counting Kit-8 reagent (Dojindo Molecular Technologies, Inc.). In brief, to each well of a 96-well plate, the cells were seeded at a density of 10,000 cells per well. Following 12 h of the seeding, the adherent cells were washed with phosphate-buffered saline and replaced with fresh 100 μl growth medium. Cell viability rate was measured every 24-hour interval, starting from 0 to 72 h, by adding 10 μl of CCK8 reagent to the appropriate groups and incubated at 37 °C for 1 h. Absorbance was quantified at a wavelength of 450 nm using a microplate reader (Molecular Devices). Cells were

[4] Please note that the JBC is not responsible for the long-term archiving and maintenance of these sites or any other third party hosted site.

seeded in triplicates for each group in this experiment and the experiment was repeated twice.

Statistical analysis

Data were represented as mean ± S.D., where $n \leq 3$. The level of significance was tested using Student's *t* test or two-way analysis of variance with Tukey's multiple comparisons test (GraphPad Prism). $p < 0.05$ was considered to be statistically significant. Tested significance is displayed in the figures as *, $p < 0.05$; **, $p < 0.01$; *** $p < 0.001$.

Author contributions—G. P. and R. N. K. B. designed the work. G. P., R. K. S., S. K. S. performed the research. G. P., M. A. I., A. B. T., and R. N. K. B. analyzed the data and wrote the paper. All authors were actively engaged in data analysis, interpretation, and drafting the manuscript.

Acknowledgment—We acknowledge Plabon Borah (Advanced Instrumentation Research Facility, Jawaharlal Nehru University, New Delhi) for providing assistance in LC-MS analysis.

References

1. Warburg, O. (1956) On the origin of cancer cells. *Science* **123,** 309–314
2. Vander Heiden, M. G., Cantley, L. C., and Thompson, C. B. (2009) Understanding the Warburg effect: The metabolic requirements of cell proliferation. *Science* **324,** 1029–1033
3. Cairns, R. A., Harris, I. S., and Mak, T. W. (2011) Regulation of cancer cell metabolism. *Nat. Rev. Cancer* **11,** 85–95
4. Christofk, H. R., Vander Heiden, M. G., Harris, M. H., Ramanathan, A., Gerszten, R. E., Wei, R., Fleming, M. D., Schreiber, S. L., and Cantley, L. C. (2008) The M2 splice isoform of pyruvate kinase is important for cancer metabolism and tumour growth. *Nature* **452,** 230–233
5. Mazurek, S. (2011) Pyruvate kinase type M2: A key regulator of the metabolic budget system in tumor cells. *Int. J. Biochem. Cell Biol.* **43,** 969–980
6. Noguchi, T., Inoue, H., and Tanaka, T. (1986) The M1- and M2-type isozymes of rat pyruvate kinase are produced from the same gene by alternative RNA splicing. *J. Biol. Chem.* **261,** 13807–13812
7. Clower, C. V., Chatterjee, D., Wang, Z., Cantley, L. C., Vander Heiden, M. G., and Krainer, A. R. (2010) The alternative splicing repressors hnRNP A1/A2 and PTB influence pyruvate kinase isoform expression and cell metabolism. *Proc. Natl. Acad. Sci. U.S.A.* **107,** 1894–1899
8. Chaneton, B., and Gottlieb, E. (2012) Rocking cell metabolism: Revised functions of the key glycolytic regulator PKM2 in cancer. *Trends Biochem. Sci.* **37,** 309–316
9. Iqbal, M. A., Gupta, V., Gopinath, P., Mazurek, S., and Bamezai, R. N. (2014) Pyruvate kinase M2 and cancer: An updated assessment. *FEBS Lett.* **588,** 2685–2692
10. Iqbal, M. A., Siddiqui, F. A., Gupta, V., Chattopadhyay, S., Gopinath, P., Kumar, B., Manvati, S., Chaman, N., and Bamezai, R. N. K. (2013) Insulin enhances metabolic capacities of cancer cells by dual regulation of glycolytic enzyme pyruvate kinase M2. *Mol. Cancer* **12,** 72
11. Mazurek, S., Boschek, C. B., Hugo, F., and Eigenbrodt, E. (2005) Pyruvate kinase type M2 and its role in tumor growth and spreading. *Semin. Cancer Biol.* **15,** 300–308
12. Gupta, V., Kalaiarasan, P., Faheem, M., Singh, N., Iqbal, M. A., and Bamezai, R. N. K. (2010) Dominant negative mutations affect oligomerization of human pyruvate kinase M2 isozyme and promote cellular growth and polyploidy. *J. Biol. Chem.* **285,** 16864–16873
13. Wong, N., Ojo, D., Yan, J., and Tang, D. (2015) PKM2 contributes to cancer metabolism. *Cancer Lett.* **356,** 184–191
14. Luo, W., Hu, H., Chang, R., Zhong, J., Knabel, M., O'Meally, R., Cole, R. N., Pandey, A., and Semenza, G. L. (2011) Pyruvate kinase M2 is a PHD3-stimulated coactivator for hypoxia-inducible factor 1. *Cell* **145,** 732–744
15. Yang, W., Xia, Y., Ji, H., Zheng, Y., Liang, J., Huang, W., Gao, X., Aldape, K., and Lu, Z. (2011) Nuclear PKM2 regulates β-catenin transactivation upon EGFR activation. *Nature* **480,** 118–122
16. Azoitei, N., Becher, A., Steinestel, K., Rouhi, A., Diepold, K., Genze, F., Simmet, T., and Seufferlein, T. (2016) PKM2 promotes tumor angiogenesis by regulating HIF-1α through NF-κB activation. *Mol. Cancer* **15,** 3
17. Gao, X., Wang, H., Yang, J. J., Liu, X., and Liu, Z. R. (2012) Pyruvate kinase M2 regulates gene transcription by acting as a protein kinase. *Mol. Cell* **45,** 598–609
18. Yang, W., Xia, Y., Hawke, D., Li, X., Liang, J., Xing, D., Aldape, K., Hunter, T., Alfred Yung, W. K., and Lu, Z. (2012) PKM2 phosphorylates histone H3 and promotes gene transcription and tumorigenesis. *Cell* **150,** 685–696
19. Jiang, Y., Li, X., Yang, W., Hawke, D. H., Zheng, Y., Xia, Y., Aldape, K., Wei, C., Guo, F., Chen, Y., and Lu, Z. (2014) PKM2 regulates chromosome segregation and mitosis progression of tumor cells. *Mol. Cell* **53,** 75–87
20. Goldberg, M. S., and Sharp, P. A. (2012) Pyruvate kinase M2-specific siRNA induces apoptosis and tumor regression. *J. Exp. Med.* **209,** 217–224
21. Chu, B., Wang, J., Wang, Y., and Yang, G. (2015) Knockdown of PKM2 induces apoptosis and autophagy in human A549 alveolar adenocarcinoma cells. *Mol. Med. Rep.* **12,** 4358–4363
22. Sun, H., Zhu, A., Zhang, L., Zhang, J., Zhong, Z., and Wang, F. (2015) Knockdown of PKM2 suppresses tumor growth and invasion in lung adenocarcinoma. *Int. J. Mol. Sci.* **16,** 24574–24587
23. Anastasiou, D., Yu, Y., Israelsen, W. J., Jiang, J. K., Boxer, M. B., Hong, B. S., Tempel, W., Dimov, S., Shen, M., Jha, A., Yang, H., Mattaini, K. R., Metallo, C. M., Fiske, B. P., Courtney, K. D., *et al.* (2012) Pyruvate kinase M2 activators promote tetramer formation and suppress tumorigenesis. *Nat. Chem. Biol.* **8,** 839–847
24. Parnell, K. M., Foulks, J. M., Nix, R. N., Clifford, A., Bullough, J., Luo, B., Senina, A., Vollmer, D., Liu, J., McCarthy, V., Xu, Y., Saunders, M., Liu, X. H., Pearce, S., Wright, K., O'Reilly, M., McCullar, M. V., Ho, K. K., and Kanner, S. B. (2013) Pharmacologic activation of PKM2 slows lung tumor xenograft growth. *Mol. Cancer Ther.* **12,** 1453–1460
25. Walsh, M. J., Brimacombe, K. R., Anastasiou, D., Yu, Y., Israelsen, W. J., Hong, B. S., Tempel, W., Dimov, S., Veith, H., Yang, H., Kung, C., Yen, K. E., Dang, L., Salituro, F., Auld, D. S., Park, H. W., Vander Heiden, M. G., Thomas, C. J., Shen, M., and Boxer, M. B. (2010) ML265: A potent PKM2 activator induces tetramerization and reduces tumor formation and size in a mouse xenograft model. In *Probe Reports from the NIH Molecular Libraries Program* (online), National Center for Biotechnology Information, Bethesda, MD
26. Cortés-Cros, M., Hemmerlin, C., Ferretti, S., Zhang, J., Gounarides, J. S., Yin, H., Muller, A., Haberkorn, A., Chene, P., Sellers, W. R., and Hofmann, F. (2013) M2 isoform of pyruvate kinase is dispensable for tumor maintenance and growth. *Proc. Natl. Acad. Sci. U.S.A.* **110,** 489–494
27. Israelsen, W. J., Dayton, T. L., Davidson, S. M., Fiske, B. P., Hosios, A. M., Bellinger, G., Li, J., Yu, Y., Sasaki, M., Horner, J. W., Burga, L. N., Xie, J., Jurczak, M. J., DePinho, R. A., Clish, C. B., *et al.* (2013) PKM2 isoform-specific deletion reveals a differential requirement for pyruvate kinase in tumor cells. *Cell* **155,** 397–409
28. Faubert, B., Vincent, E. E., Griss, T., Samborska, B., Izreig, S., Svensson, R. U., Mamer, O. A., Avizonis, D., Shackelford, D. B., Shaw, R. J., and Jones, R. G. (2014) Loss of the tumor suppressor LKB1 promotes metabolic reprogramming of cancer cells via HIF-1α. *Proc. Natl. Acad. Sci. U.S.A.* **111,** 2554–2559
29. Shackelford, D. B., Abt, E., Gerken, L., Vasquez, D. S., Seki, A., Leblanc, M., Wei, L., Fishbein, M. C., Czernin, J., Mischel, P. S., and Shaw, R. J. (2013) LKB1 inactivation dictates therapeutic response of non-small cell lung cancer to the metabolism drug phenformin. *Cancer cell* **23,** 143–158
30. Ji, H., Ramsey, M. R., Hayes, D. N., Fan, C., McNamara, K., Kozlowski, P., Torrice, C., Wu, M. C., Shimamura, T., Perera, S. A., Liang, M. C., Cai, D., Naumov, G. N., Bao, L., Contreras, C. M., *et al.* (2007) LKB1 modulates lung cancer differentiation and metastasis. *Nature* **448,** 807–810
31. Jiang, W., Hua, R., Wei, M., Li, C., Qiu, Z., Yang, X., and Zhang, C. (2015) An optimized method for high-titer lentivirus preparations without ultracentrifugation. *Sci. Rep.* **5,** 13875

32. Qin, X., Du, Y., Chen, X., Li, W., Zhang, J., and Yang, J. (2014) Activation of Akt protects cancer cells from growth inhibition induced by PKM2 knockdown. *Cell Biosci.* **4,** 20
33. Jenkins, C. M., Yang, J., Sims, H. F., and Gross, R. W. (2011) Reversible high affinity inhibition of phosphofructokinase-1 by acyl-CoA: A mechanism integrating glycolytic flux with lipid metabolism. *J. Biol. Chem.* **286,** 11937–11950
34. Colombo, G., Tate, P. W., Girotti, A. W., and Kemp, R. G. (1975) Interaction of inhibitors with muscle phosphofructokinase. *J. Biol. Chem.* **250,** 9404–9412
35. Zhang, M., Zhu, H., Ding, Y., Liu, Z., Cai, Z., and Zou, M. H. (2017) AMP-activated protein kinase α1 promotes atherogenesis by increasing monocyte-to-macrophage differentiation. *J. Biol. Chem.* **292,** 7888–7903
36. Kim, J., Kundu, M., Viollet, B., and Guan, K. L. (2011) AMPK and mTOR regulate autophagy through direct phosphorylation of Ulk1. *Nat. Cell Biol.* **13,** 132–141
37. Marcus, A. I., and Zhou, W. (2010) LKB1 regulated pathways in lung cancer invasion and metastasis. *J. Thorac. Oncol.* **5,** 1883–1886
38. Hezel, A. F., and Bardeesy, N. (2008) LKB1; linking cell structure and tumor suppression. *Oncogene* **27,** 6908–6919
39. Carretero, J., Medina, P. P., Blanco, R., Smit, L., Tang, M., Roncador, G., Maestre, L., Conde, E., Lopez-Rios, F., Clevers, H. C., and Sanchez-Cespedes, M. (2007) Dysfunctional AMPK activity, signalling through mTOR and survival in response to energetic stress in LKB1-deficient lung cancer. *Oncogene* **26,** 1616–1625
40. Dupuy, F., Griss, T., Blagih, J., Bridon, G., Avizonis, D., Ling, C., Dong, Z., Siwak, D. R., Annis, M. G., Mills, G. B., Muller, W. J., Siegel, P. M., and Jones, R. G. (2013) LKB1 is a central regulator of tumor initiation and pro-growth metabolism in ErbB2-mediated breast cancer. *Cancer Metabol.* **1,** 18
41. Inge, L. J., Coon, K. D., Smith, M. A., and Bremner, R. M. (2009) Expression of LKB1 tumor suppressor in non-small cell lung cancer determines sensitivity to 2-deoxyglucose. *J. Thorac. Cardiovasc. Surg.* **137,** 580–586
42. Whang, Y. M., Park, S. I., Trenary, I. A., Egnatchik, R. A., Fessel, J. P., Kaufman, J. M., Carbone, D. P., and Young, J. D. (2016) LKB1 deficiency enhances sensitivity to energetic stress induced by erlotinib treatment in non-small-cell lung cancer (NSCLC) cells. *Oncogene* **35,** 856–866
43. Hardie, D. G., and Alessi, D. R. (2013) LKB1 and AMPK and the cancer-metabolism link–ten years after. *BMC Biol.* **11,** 36
44. Shackelford, D. B., and Shaw, R. J. (2009) The LKB1-AMPK pathway: Metabolism and growth control in tumour suppression. *Nat. Rev. Cancer* **9,** 563–575
45. Hardie, D. G., Ross, F. A., and Hawley, S. A. (2012) AMPK: A nutrient and energy sensor that maintains energy homeostasis. *Nat. Rev. Mol. Cell Biol.* **13,** 251–262
46. Pal, R., Gochhait, S., Chattopadhyay, S., Gupta, P., Prakash, N., Agarwal, G., Chaturvedi, A., Husain, N., Husain, S. A., and Bamezai, R. N. (2011) Functional implication of TRAIL −716 C/T promoter polymorphism on its *in vitro* and *in vivo* expression and the susceptibility to sporadic breast tumor. *Breast Cancer Res. Treat.* **126,** 333–343
47. Pal, R., Srivastava, N., Chopra, R., Gochhait, S., Gupta, P., Prakash, N., Agarwal, G., and Bamezai, R. N. K. (2010) Investigation of DNA damage response and apoptotic gene methylation pattern in sporadic breast tumors using high throughput quantitative DNA methylation analysis technology. *Mol.Cancer* **9,** 303
48. Chu, C., Xin, A., Zhou, Y., and Zhang, Y. (2013) A simple protocol for producing high-titer lentivirus. *Acta Biochim. Biophys. Sin.* **45,** 1079–1082
49. David, C. J., Chen, M., Assanah, M., Canoll, P., and Manley, J. L. (2010) HnRNP proteins controlled by c-Myc deregulate pyruvate kinase mRNA splicing in cancer. *Nature* **463,** 364–368
50. Yu, C. S., Lin, C. J., and Hwang, J. K. (2004) Predicting subcellular localization of proteins for Gram-negative bacteria by support vector machines based on n-peptide compositions. *Protein Sci.* **13,** 1402–1406
51. Yu, C. S., Chen, Y. C., Lu, C. H., and Hwang, J. K. (2006) Prediction of protein subcellular localization. *Proteins* **64,** 643–651
52. Garg, A., Bhasin, M., and Raghava, G. P. S. (2005) SVM-based method for subcellular localization of human proteins using amino acid compositions, their order and similarity search. *J. Biol. Chem.* **280,** 14427–14432
53. Shen, H.-B., and Chou, K.-C. (2009) A top-down approach to enhance the power of predicting human protein subcellular localization: Hum-mPLoc 2.0. *Anal. Biochem.* **394,** 269–274
54. Shen, H.-B., and Chou, K.-C. (2007) Hum-mPLoc: An ensemble classifier for large-scale human protein subcellular location prediction by incorporating samples with multiple sites. *Biochem. Biophys. Res. Commun.* **355,** 1006–1011
55. Chen, H., Huang, N., and Sun, Z. (2006) SubLoc: A server/client suite for protein subcellular location based on SOAP. *Bioinformatics* **22,** 376–377
56. Briesemeister, S., Rahnenführer, J., and Kohlbacher, O. (2010) Going from where to why—interpretable prediction of protein subcellular localization. *Bioinformatics* **26,** 1232–1238
57. Briesemeister, S., Rahnenführer, J., and Kohlbacher, O. (2010) YLoc—an interpretable web server for predicting subcellular localization. *Nucleic Acids Res.* **38,** W497–W502
58. Pierleoni, A., Martelli, P. L., Fariselli, P., and Casadio, R. (2006) BaCelLo: A balanced subcellular localization predictor. *Bioinformatics* **22,** e408–e416